AIAA 80-1206R

Flame Propagation and Combustion Processes in Solid Propellant Cracks

Mridul Kumar,* Stephen M. Kovacic,† and Kenneth K. Kuo‡
The Pennsylvania State University, University Park, Penn.

The effects of pressurization rate, crack-gap width, crack length, and propellant type on the ignition and flame-spreading processes in isolated AP-based solid propellant cracks have been studied experimentally. Ignition front propagation rates were measured using a high-speed (up to 44,000 pictures/s) camera. Cracks up to 200 mm in length with gap widths as low as 450 μm were studied. It was observed that the hot gases precede the ignition front. The ignition-front propagation speed increases near the crack entrance, reaches a maximum, and then decreases near the crack tip. The results of parametric study indicate that the time required for the ignition front to reach the crack tip decreases, and that the maximum velocity of the ignition front increases as the pressurization rate or burning rate of the propellant is increased. The maximum pressure in the crack increases with an increase in burning rate or crack length, but decreases with an increase in gap width.

Nomenclature

a = pre-exponential factor in Saint Robert's burning rate relationship aP^n, (mm/s)/(atm)^n
An = Andreev number, $r_b d_h/\alpha$
d_h = hydraulic diameter of crack, mm
L = length of crack, mm
n = pressure exponent in Saint Robert's burning rate relationship
P = pressure, atm
P_{max} = maximum pressure in the crack cavity, atm
r_b = burning rate of solid propellant, mm/s
T = temperature, K
t = time, s
T_f = adiabatic flame temperature of solid propellant, K
T_{pi} = initial propellant temperature, 295 K
v_{fp} = convective ignition front propagation velocity, m/s
x = axial location, measured from entrance of crack, mm
α = thermal diffusivity
δ = gap width of crack
ρ = density, kg/m^3

Introduction

UNDER certain operating conditions, high-pressure and high-temperature gases from the rocket chamber penetrate the defects or cracks that are present in solid propellants. The convective heat transfer from the hot gases heats the propellants along the cracks, and if a sufficient amount of energy is transferred to the propellants, ignition also occurs inside the defects. Burning inside defects or cavities may result in much higher pressures in the cavities; indeed, it is believed that given the proper stimuli, these defects or multiple cracks may initiate detonation. Even if this abnormal burning does not lead to a catastrophic failure, it may cause the performance of the rocket motor to deviate significantly from the designed conditions.

Presented as Paper 80-1206 at the AIAA/SAE/ASME 16th Joint Propulsion Conference, Hartford, Conn., June 30-July 2, 1980; submitted July 31, 1980; revision received Dec. 22, 1980.

*Assistant Professor, Department of Mechanical Engineering. Member AIAA.
†Graduate Student, presently working at TRW Ballistic Missiles Division, San Bernadino, Calif.
‡Associate Professor, Department of Mechanical Engineering. Associate Fellow AIAA.

This paper deals with a detailed experimental investigation of the development of convective burning in an isolated propellant crack. Convective burning is defined as enhanced burning of a propellant charge, caused by hot gas penetration into propellant defects. Forced convection is the primary heat transfer mechanism during convective burning. Even though the ignition, flame spreading, and combustion processes inside an isolated solid propellant crack represent an idealized case of the actual burning in propellant defects, a fundamental understanding of the ignition and flame-propagation processes in such a geometry is essential in order to study the extremely complex phenomenon of ignition in defects, leading to deflagration-to-detonation transition (DDT). It should be noted, however, that a single crack will result in a limited increase in burning surface area, and, therefore, may not cause detonation.

Prior to this study several researchers have investigated convective burning in solid propellant defects. Recently, Bradley and Boggs[1] have made an extensive literature review on convective burning in propellant defects. Belyaev et al.[2] have compiled most of the recent work done in this area in the USSR. These reviews indicate that the convective burning in solid propellant cracks has been investigated by a number of researchers in the past and that both theoretical and experimental techniques have been used. Studies in this area have also been conducted at The Pennsylvania State University.[3-7] Experimental studies on convective burning in solid propellant cracks can be subdivided into two broad categories[1,2]: 1) onset of convective burning, and 2) development of convective burning. Literature on the onset of convective burning is extensive; the studies are usually qualitative in nature and are characterized by tests of the go/no-go type. Results of studies on the onset of combustion are commonly presented in graphical form to indicate the operating conditions (usually pressure) under which the flame will penetrate a crack of a given dimension. The following paragraphs list some of the important work in this area.

Prentice[8] conducted experimental investigations on the onset of convective burning in a transparent, nitrocellulose-petrin propellant. He observed that it was much easier to flashdown into a crack with both ends open than into a crack with one end closed. Catalytic additives caused flashdown to occur more readily. Flashdown was not observed up to 3.9 MPa in 1.6-mm-diam cracks. Both motion pictures and thermocouples were used to monitor flame penetration. Later, Prentice[9] extended his work to opaque composite propellants. Vibration response spectroscopy (VRS) was used to monitor flashdown. Double-based propellants that displayed mesa burning were also investigated by Prentice. He

concluded that the critical pore diameter for flashdown in a given propellant is inversely proportional to the burning rate. Margolin and Margulis[10] noted that combustion penetrates more easily into a channel with two open ends than into a blind channel. They also observed that if the channel were open at one end, or if there were one or more outlets from the channel to the burning surface, the combustion gases instantaneously penetrated the pores when the Andreev number (An) was beyond a critical value. However, the critical Andreev number is not always constant.

Godai[11] made experimental investigations of flame propagation in the narrow slit and fine hole of solid propellant grain. Cracks of 22 mm in length were formed with 5 mm square slabs of AP-based composite propellants. The propellant was ignited with a nichrome wire, and the ignition event was filmed by motion-picture camera at a rate of about 32 frames/s. Tests were conducted in a slab of propellant with both a single hole and multiple holes. Godai observed that there is a threshold gap width or hole diameter below which the flame does not propagate into the defect, and that the threshold crack gap is fundamentally a function of the burning rate. Bobolev et al.,[12] Payne,[13] and Krasnov et al.[14] also studied the onset of convective burning in solid propellant cracks.

Experimental studies on the development of convective burning are limited. Belyaev et al.[15,16] made preliminary investigations of the development of combustion in single pores. The flame propagation rate was observed to increase initially, and then to reach a constant value. The pressure in the crack was found to be greater than that of the chamber, and the effect of erosive burning was found to be important. The maximum pressure in the crack was correlated with the crack length and the ratio of the crack length to crack width.

The focus of previous investigations of combustion in propellant cracks has been on the onset of convective burning; the development of convective burning has yet to be investigated fully. It is generally believed that the development of convective burning in a propellant defect is a necessary condition for subsequent transition to detonation. Almost all of the previous studies have been conducted at constant pressure conditions. The effect of chamber pressurization rate (dP/dt) on flame propagation, which is of interest in actual rocket motor and DDT studies, has not yet been investigated.

The aim of the present research was to narrow some of the technological gaps that exist in the study of the development of convective burning in solid propellant cracks. The specific objectives of this investigation are:

1) To experimentally study the effect of the following parameters on ignition and flame propagation inside Ammonium-Perchlorate-based composite solid propellant cracks: a) chamber pressurization rate, b) crack gap width, c) length of the crack, and d) propellant composition.

2) To establish a data base for the convective flame-propagation rate and the maximum pressure in the crack cavity as a function of pressurization rate, crack geometry, and the physicochemical properties of the propellant.

The results of this study can also be used for verification purposes, in order to compare the flame-propagation rates and pressure measurements along axial locations of the crack, with the numerical predictions of a parallel theoretical study being conducted by the authors at The Pennsylvania State University.

Experimental Setup and Procedures

Test Apparatus

The test apparatus and experimental conditions for this study incorporated the following major design considerations: 1) the test apparatus should allow a wide range of variation in crack geometry and operating conditions; and 2) test conditions should simulate, as closely as possible, those in an actual rocket motor. A solid propellant igniter system (details of which are given in the following section) was used

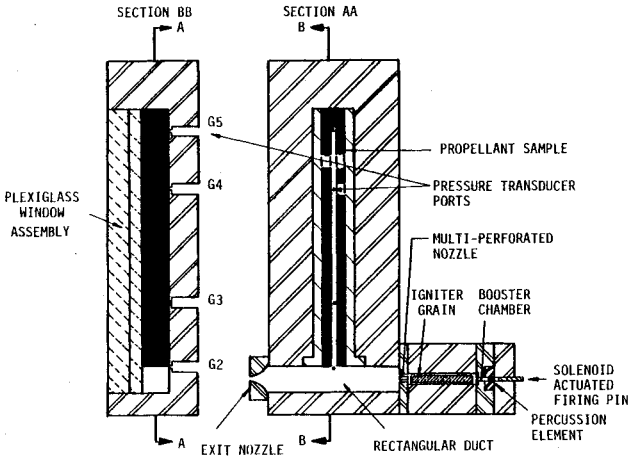

Fig. 1 Schematic diagram of combustion chamber.

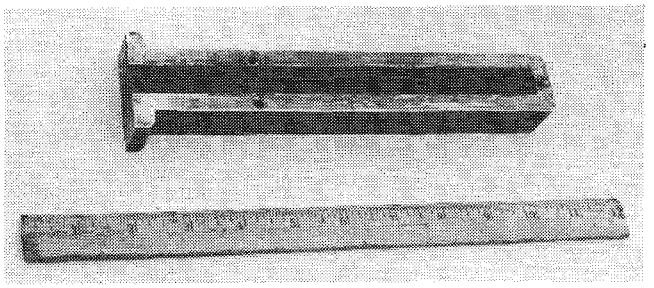

Fig. 2 Typical propellant crack sample.

to simulate igniter gas composition similar to that in an actual rocket motor. Using this igniter system, it was possible to obtain pressures up to 200 atm in the chamber in approximately 2 ms. The test apparatus is also compatible with the theoretical model developed by the authors[5,17] and, therefore, the results obtained here could later be used for model validation.

Igniter System

A solid propellant igniter system was the source for hot gas generation. Percussion primers were used as initiators for ignition of a propellant charge. A remotely controlled, solenoid-activated firing pin was used to trigger the primer. A schematic diagram of the test chamber and igniter system is shown in Fig. 1. The igniter system consists of 1) a solenoid mounted on the retainer block of a spring-loaded firing pin, 2) a percussion element and its housing unit, 3) a propellant igniter charge and igniter chamber, and 4) a multiperforated nozzle plate. All hardware was made of stainless steel.

High-temperature, high-velocity gases, under rapidly increasing pressure conditions that simulate flow conditions in a rocket chamber, were obtained by burning a 50 mm long, rectangular cross-sectional ($\sim 5.7 \times 5.7$ mm) solid propellant charge. This charge was placed inside the cavity of the igniter chamber; the diameter of the cavity is 8 mm. When the primer was triggered, it produced hot gases which flowed over and ignited the solid propellant charge. The product gases flowed through a multiperforated converging nozzle into the main chamber. The pressurization rate of the chamber can be varied by altering the dimensions of the propellant strip in the igniter, by changing the dimensions of the multiperforated nozzle, or by changing the exit nozzle of the chamber.

Test Chamber and Crack Configurations

The test chamber shown in Fig. 1 was made of stainless steel 304. The discharge of the igniter system passes through a 124 mm long, rectangular cross-sectional (10×25.4 mm) channel. The propellant crack sample is placed perpendicular

to the flow direction in the main chamber. Cracks were formed by cutting a slot of desired width in a propellant slab (of 25.4 × 17 mm cross section) glued into a brass retainer. It was possible to manufacture cracks up to 210 mm in length, with gap widths as low as 450 μm. Figure 2 shows a typical propellant crack sample. Four pressure ports were provided along the center of the crack in order to measure pressure variation along the crack. An interchangeable, convergent exit nozzle was used to vary pressure and flow conditions in the chamber. The nozzle was made of titanium in order to alleviate the problem of metal erosion caused by highly corrosive gases. The exit diameter of the nozzle was varied between 2.5 and 3.8 mm. For safety, the chamber was also equipped with a port for a burst diaphragm. If for any reason pressure inside the chamber exceeded a predetermined value (usually 680 atm), the burst diaphragm would rupture to vent pressure and avoid an explosion.

Flame propagation in the crack was observed through a set of transparent plexiglass windows. The window assembly consisted of a sacrificial window (238 × 65 × 6.3 mm) and a viewing window (251 × 78 × 25.4 mm). The window assembly was held in place by a stainless steel window retainer. To achieve a good seal, rubber O-rings were used between the two halves of the chamber, and between the inlet and exit nozzles and the chamber. During the tests, the chamber was completely sealed, except for the interchangeable exit nozzle through which product gases were discharged into the atmosphere. Since the sacrificial window is placed directly over the propellant surface, it is destroyed after each test firing. The test sample is clearly visible through the windows during the test.

To obtain a more detailed observation of the flame-front propagation, an alternative crack sample shown in Fig. 3 was used to replace the one shown in Fig. 2. The alternative crack sample provided direct (front view) observation of the gas penetration and ignition-front propagation processes. In this configuration, the crack was formed between a propellant slab and the sacrificial plexiglass window, i.e., one side of the crack was an inert, transparent, plexiglass window and the other side was a propellant slab glued to a stainless steel base plate. The gap width of such a crack configuration is varied by the amount by which the propellant surface is recessed below the side-leg assembly (see Fig. 3). The propellant slabs for these tests were 183 mm long and 17.7 mm wide. Gap widths of the crack were varied between 0.43 and 1.5 mm. It should be noted that for this configuration only two pressure traces can be obtained: one at the crack entrance, and the other at the tip.

Instrumentation

Data Acquisition System

A block diagram of the data acquisition system for the convective flame propagation studies is shown in Fig. 4. The data acquisition system consists of three major parts: 1) pressure measuring system, 2) flame propagation measuring system, and 3) transient waveform recording system. Details of measurement techniques are given in the following sections. The data acquisition system includes: pressure transducers, charge amplifiers, a high-speed movie camera, a light-emitting diode (LED) driving unit, a motion analyzer, a 9-channel transient waveform recorder (Physical Data Model #515.234), a 7-channel FM tape recorder, an oscilloscope and an *x-y* plotter. The maximum sampling rate of the Physical Data System is 2×10^6 samples/s, and the maximum amplitude resolution is 0.1% with a 4096 word memory per channel. The recording speed of the HP type recorder is 60 in./s at a carrier frequency of 108 kHz. The tape can be played back at a much lower speed (1⅞ in./s) to expand the duration of the transient signals. Data recorded on the Physical Data System can be displayed on an oscilloscope, or plotted on an *x-y* plotter for a hard copy. Data recorded on tape is digitized before display or plotting.

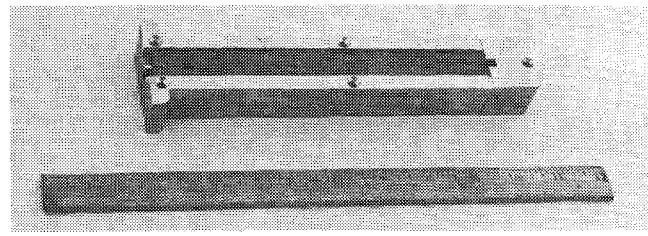

Fig. 3 Propellant sample for detailed observation of ignition front.

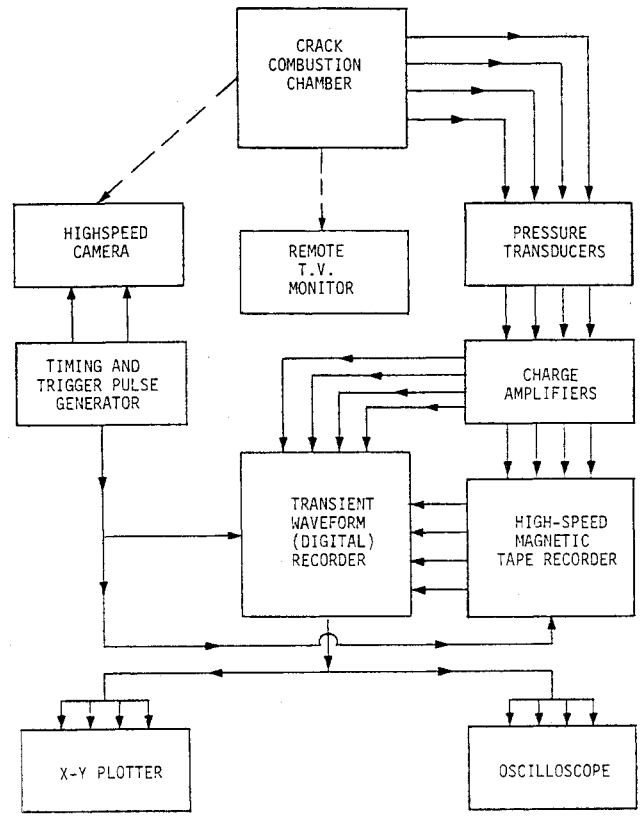

Fig. 4 Block diagram of data acquisition system.

Pressure Measurements

Four ports are provided along the length of the crack for transient pressure measurements. The first port is located in the main chamber, very close to the crack entrance. The other three are located at 48, 138, and 188 mm from the first transducer port. Piezoelectric quartz transducers were used to measure the pressure. The transducers have a rise time of 1.5 μs and a natural frequency of 300 kHz, and can accurately record pressures up to 1000 atm. The transducers were mounted in a water-cooled adapter that prevented drifting or damage due to excessive heat. In addition, a thin layer of silicon rubber insulation was placed on the transducer surface to further protect the transducer diaphragm from high-temperature gases. The transducers were mounted about 2 mm below the bottom surface of the chamber.

Charge signals from the pressure transducers were carried through an insulated, high-impedance, coaxial cable to a charge amplifier. The output (voltage signal) of the charge amplifiers was recorded simultaneously on the transient waveform recorder and on the magnetic tape. In order to accurately determine the pressure level, calibration signals equivalent to 69 atm (1000 psig) were also recorded for each channel. Calibration signals for each transducer were checked periodically by comparing them with signals obtained from measuring a known pressure of a high-pressure nitrogen or air tank.

Flame-Propagation Measurements

A high-speed, 16 mm motion picture camera was used to observe the complete ignition event in the chamber. With a quarter-frame optical head, the camera was capable of filming at a maximum of about 44,000 pictures/s. The Hycam camera is equipped with a dual light-emitting diode (LED) system; one LED records timing marks and the other records a common-time signal on the film. The common-time signal is generated at the start of the event, and is used to correlate events recorded on the transient waveform recorder or tape with those on the film. The LED driver unit, a common-time pulse and high-frequency (up to 10 kHz) timing generator, was used to operate the LED time system. The frequency of the timing pulse in the present investigation was set at 1 or 10 kHz.

The Vanguard motion analyzer was used to analyze the film, frame by frame. The motion analyzer screen is equipped with two cross hairs to traverse in two perpendicular directions in a plane. Two micrometer dials, accurate to a thousandth of an inch, are used to record the movement of the cross hairs. The analyzer's frame counter is designed to keep track of the number of frames analyzed. In order to obtain the flame-propagation speed for a fixed y location (centerline of the crack), x readings (along the crack) were taken for each frame until the flame reached the crack tip. Readings of the micrometer dials were scaled by using the known value of the initial length of the crack and the total distance traversed by the crosswire. The time interval between each picture was obtained from the time marks on the film.

Remotely Controlled Ignition Circuit

The transient ignition processes in a solid propellant crack involve high pressures and very high pressurization rates ($\sim 10^5$ atm/s). Because pressurization rates of such a magnitude are potentially hazardous, experiments were carried out in a test cell with 1½-ft thick concrete walls, and the ignition event was remotely controlled.

A block diagram of the remotely controlled ignition and high-speed photography system is shown in Fig. 5. The solenoid that triggers the percussion primer is activated by an event switch built into the high-speed camera. After the camera is switched on, about one second is required to reach the desired framing rate. This delay time can be related to the footage of the film that passes through the camera before the attainment of the prescribed framing rate. The event switch is controlled by a footage indicator. During operation, the footage indicator is set to a preselected value corresponding to the desired framing rate. For example, the indicator is set at 100 ft for a framing rate of 40,000 pictures/s. After a specified length of film (preset on the footage indicator) passes through the camera, the event switch closes, causing 12 V ac to be applied across the relay, and the relay is activated. The relay, in turn, activates two other switches; one switch triggers the solenoid (by causing a current to flow through it) and initiates the ignition event, and the other closes the common-time switch on a light-emitting diode (LED) driver unit. At the instant at which the common-time switch closes, the LED driver unit generates a 2 ms pulse that is recorded on the transient waveform recorders and is simultaneously marked on the film. These common-time marks are used for time correlation of the data recorded on the tape and film.

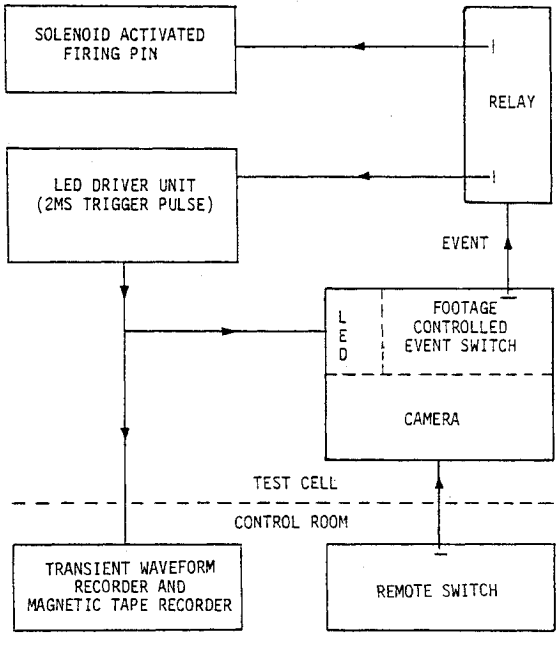

Fig. 5 Block diagram of remotely controlled ignition and photography system.

Test Procedure

Test samples were prepared from cast propellant grains obtained from propellant processing laboratories. Propellant slabs (approximately 215 × 26 × 17 mm) were cut from the cast propellant with a remotely controlled milling machine. A slightly oversized propellant slab was glued into a brass retainer. The sample was left to dry for 24 h in order to achieve a good adhesive bond between the propellant and the brass retainer. The sample was machined again to the desired dimensions. A crack of the desired dimension was then precisely cut through the center of the crack sample with a jeweler's slitting saw. Propellant samples for the alternative configuration (for detailed flame-front observation) were obtained in a similar manner. Oversized propellant slabs were glued onto a steel plate and machined to the desired dimensions. The entrance region of the crack was rounded slightly to ensure smooth flow development inside the crack. After machining, the samples were carefully cleaned with a high-pressure air jet to remove any loose particles in the crack cavity.

During assembly of the test chamber, a part of the propellant side surface in contact with the sacrificial plexiglass window and the combustion chamber was coated with a thin layer of flame retardant to help prevent the flame from penetrating between the propellant and the contact surfaces. A layer of rubber-based adhesive sealant was applied to all contact surfaces of the various components of the test chamber to prevent leaks during experiments. After the crack sample was mounted into the crack combustion chamber, the crack geometry was carefully measured and recorded. High-intensity camera lights were used during the test to facilitate motion-picture recording. In order to observe the ignition event remotely and to detect possible leaks during the test, a video monitor with a TV camera was used.

Results and Discussion

Four types of AP-based composite solid propellants were used in this investigation. Table 1 lists the propellants and some of their properties. Propellants A and B have almost identical pressure exponents in the Saint Robert's burning rate relationship; however, propellant A has a higher burning rate since it has a larger pre-exponential factor. Propellant B (AP/PBAA-EPON) was used in most of the tests. Propellants C and D have identical binder (HTPB) and oxidizer weight fractions (73%); however, the oxidizer particle size in propellant C is 20 μm, whereas the oxidizer particle size in propellant D is 200 μm. The effect of oxidizer particle size on the ignition and flame propagation processes can be obtained from a comparison of the results of these two propellants.

The physical processes that take place during the test can be described generally as follows. Discharge of product gases from the igniter system pressurizes the test chamber, causing hot ignition gases to penetrate the crack cavity. The pressure-wave fronts move along the crack, and the hot gases transfer

Table 1 Propellant properties

Propellant type	A	B	C	D
Composition	AP-based	AP/PBAA-EPON	AP/HTPB	AP/HTPB
Weight percent of oxidizer	...[a]	75	73	73
Average particle size d_{AP}, μm	...[a]	76	20	200
Pre-exponential factor in Saint Robert's burning rate expression a, mm/s/(atm)^n	1.62	0.9591	0.8441	0.5849
Pressure exponent in Saint Robert's burning rate expression, n	0.4108	0.41	0.5611	0.5427
Flame temperature T_f, K	3000	1920	1667	1667
Propellant density, kg/m^3	1710	1600	1492	1492

[a] AP weight percent and particle size for propellant A not available to the authors.

heat to the crack surface, resulting in an increase in propellant surface temperature. As the pressure in the chamber continues to increase, more hot gases are driven into the crack, and there is also an increase in the convective heat-transfer rate. Eventually, the ignition condition is realized, and the propellant begins to burn. Following the flame-spreading period, the gasification of the crack surface may generate a pressure higher than that in the chamber. Finally, the gases flow out of the crack into the main chamber.

As mentioned in the section on instrumentation, pressure measurements were made at four axial locations along the crack. The ignition-front propagation speed was deduced from films of the flame-front propagation made by a high-speed camera. Because of the complexity involved with accurate quantitative measurement of temperature for highly transient flow situations, no attempt was made to measure the temperature in the crack. (The time required for the flame to propagate from the crack entrance to the crack tip was less than 1 ms in most cases.) High gas temperatures also make this kind of measurement difficult. In all test firings the initial pressure in the crack chamber was 1 atm, and the initial temperature of the propellant was about 295 K. Results of pressure and flame-propagation measurements are discussed next, followed by results of the parametric study.

A typical set of time-correlated pressure traces is shown in Fig. 6. In this figure a dual time base is used to obtain maximum information in one plot. The initial portions of the *P-t* traces have been expanded to illustrate the pressurization processes at various locations along the crack. Gage G2 is located at the crack entrance, and G5 near the crack tip. The qualitative nature of the curves is similar, with the following important differences: 1) the first discernible pressure rise for each pressure gage occurred consecutively from the crack entrance to the crack tip, i.e., from G2 to G5; 2) the pressurization rate increased consecutively downstream from the crack entrance; and 3) the maximum pressure occurred in the interior of the crack. The time delay between the first discernible pressure rise at downstream locations and that at the crack entrance is caused by the finite time required for the hot product gases to travel from the entrance to the tip during initial pressurization. The increase in pressurization rate at downstream locations is caused by the coalescence of the traveling pressure waves. This can be further explained by noting that as the igniter is discharged, the pressure of the chamber rises, causing weak pressure waves to travel downstream of the crack. As the pressure waves travel down the crack, they are followed by stronger pressure waves caused by rapidly increasing pressure in the chamber. At the same time, some of the propellant in the upstream region begins to gasify, thus creating higher pressure behind the pressure front. The result of the combined effect of the high pressure regions behind the front is a steepening of the pressure front as it moves downstream.

The pressure trace at any location can be subdivided into three regions: 1) the initial rapid pressurization region, which is controlled mainly by chamber conditions; 2) the slowly rising pressure region; and 3) the depressurization region. The initial uprising portion of the pressure-time trace is quite linear. In most cases, the flame reaches the crack tip during the initial uprising portion of pressure-time trace at the tip. Pressure in regions 2 and 3 is controlled by combustion and flow processes in the crack. As the burning of the propellant in the crack continues, the pressure in the cavity rises above that at the crack opening; later, this pressure difference causes the gases to flow out of the crack. Pressure in the crack continues to rise until the mass flow rate of the gases from the crack is greater than that generated by the burning of the propellant in the cavity. Since the pressure in this region is governed by combustion processes inside the crack, and because gage G2 is located at the crack opening in the main chamber, the highest peak pressure occurs in the interior of the crack. Depressurization is caused by the increase in crack cavity volume, as well as by the enlargement of the crack opening, but the burning surface area remains constant.

The common-time signal, which is used to correlate pressure measurement and film, is not shown in Fig. 6 because of the 10-12 ms time lag between the common-time signal and first discernible pressure rise at the crack entrance location. In order to include the common-time signal, pressure-time traces would have to be compressed substantially, which is not desirable. The time-correlated pressure and ignition data

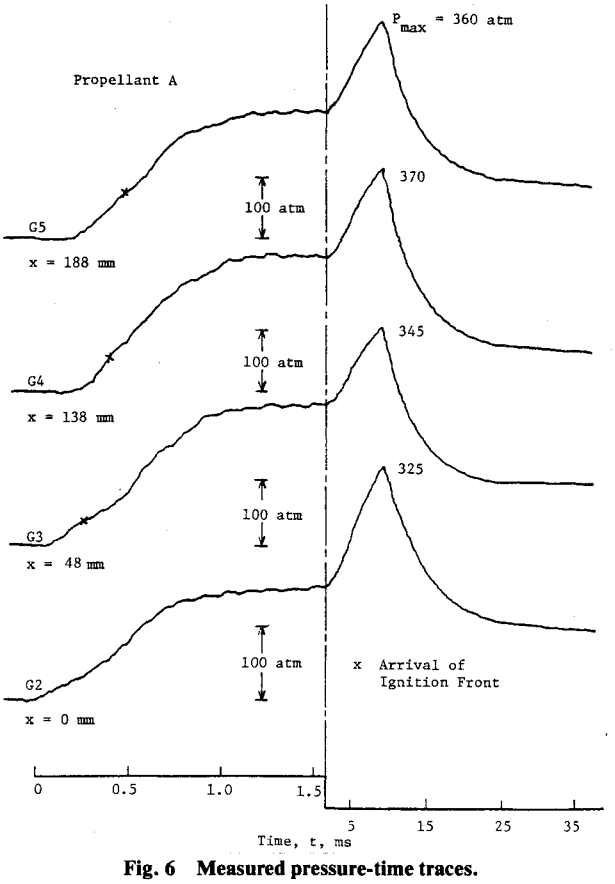

Fig. 6 Measured pressure-time traces.

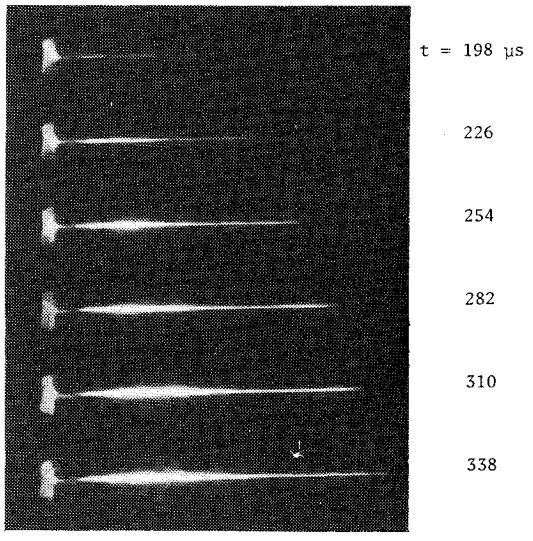

Fig. 7 Photographs of ignition front location for a typical crack test.

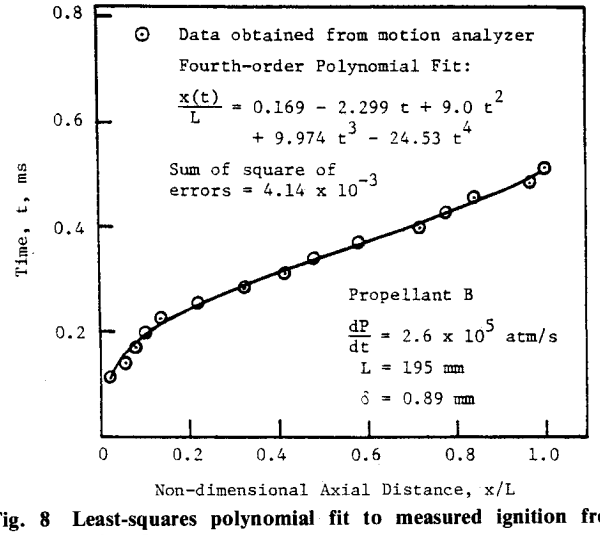

Fig. 8 Least-squares polynomial fit to measured ignition front location vs time data.

indicate that the appearance of hot igniter gases at the crack entrance coincides with the first discernible pressure rise at that point. Therefore, the initial time $t=0$ in this study can be defined as either the first discernible pressure rise at the crack entrance location, or the first appearance of hot gases on the film.

Figure 7 shows typical continuous photographs of the ignition-front propagation in a crack. The instantaneous location of the ignition front x was obtained by analyzing the film of the ignition event on a motion-picture analyzer, as discussed in the last section. The time marks on the film were used to determine the time t corresponding to each reading. A least-squares polynomial was fitted to the x-t data, and an analytic derivative of this curve was used to obtain the ignition-front propagation rate ($v_{fp}=dx/dt$). This procedure made it possible to obtain flame-propagation rates from the measured ignition-front locations. Polynomials between the third and fifth order were used, and the polynomial with the best fit was chosen to represent the analytic function relating the instantaneous flame-front location to time. Figure 8 shows a typical fourth-order polynomial fit to the measured ignition-front location vs time data. As can be seen from this figure, the curve fits the data quite well. The sum of the square of errors for this polynomial fit is 4.143×10^{-3}. In this paper, the remainder of the figures of ignition-front location vs axial distance show only the fitted polynomial. Errors are of the same order as that given in Fig. 8.

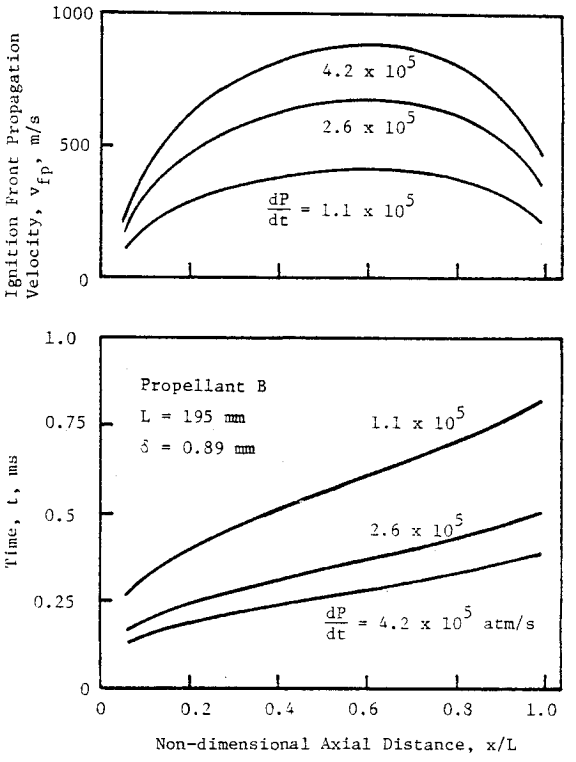

Fig. 9 Effect of pressurization rate on measured ignition front propagation.

The effect of chamber-pressurization rate on location and velocity of the ignition front for propellant B is shown in Fig. 9. The crack specimen was 195 mm long, and the gap width was 0.89 mm. The time for the flame to propagate to a given axial location and the velocity of the ignition front at that location are plotted as a function of the nondimensional axial coordinate for pressurization rates of 1.1×10^5, 2.6×10^5, and 4.2×10^5 atm/s. The time required for the flame to reach the crack tip is 836, 511, and 391 μs, respectively. That is, as the chamber pressurization rate increases, the ignition front propagates much more quickly into the crack because the rapidly increasing pressure in the chamber acts as the driving force for the penetration of hot gases into the crack. This higher pressurization causes an increase in the velocity of the gas flowing into the crack, and results in a higher rate of heat transfer to the crack walls. Faster ignition-front propagation is a net effect of these conditions. It should be noted that because of the presence of bright gases near the crack entrance, it is extremely difficult to identify the time at which the ignition front at the crack opening first appears. This explains why the plots do not show data near $x=0$.

It is interesting to note that the nature of the curves is the same in all three cases. By extrapolating the time vs axial location curve to $x=0$, the time lag between the arrival of hot gases in the chamber and the initiation of the ignition front near the crack entrance is evident. The time lag decreases as the pressurization rate is increased. The ignition-front velocity vs the nondimensional axial coordinate curve shows that after the ignition front is created near the crack entrance, it accelerates, reaches a maximum, and then decelerates. This deceleration near the closed end is more pronounced with a higher pressurization rate. At a low pressurization rate, the velocity remains relatively uniform over the bulk of the crack length. Initial acceleration is caused by the preheating by the hot gases that precede the ignition front. Deceleration is believed to be caused by the end effects. Deceleration of the ignition front is in agreement with the observation made by Taylor[18] concerning ignition of granular propellants with a closed-end boundary. Maximum ignition-front propagation velocities are 410, 675, and 886 m/s for the pressurization rates of 1.1×10^5, 2.6×10^5, and 4.2×10^5 atm/s, respec-

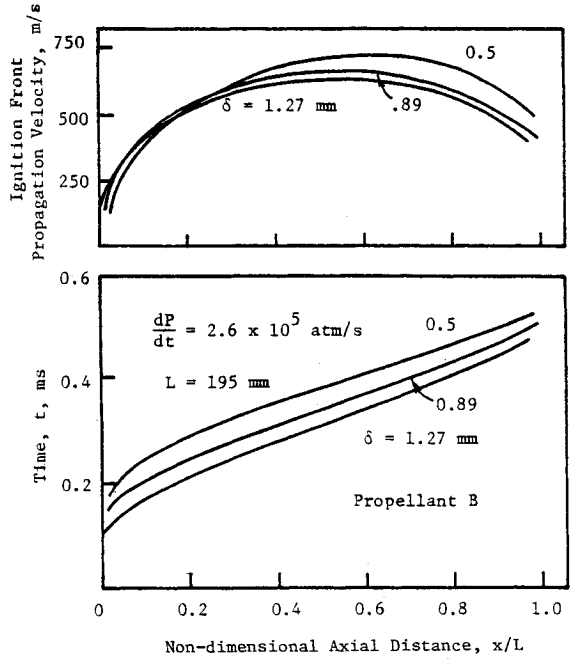

Fig, 10 Effect of gap width on measured ignition front propagation.

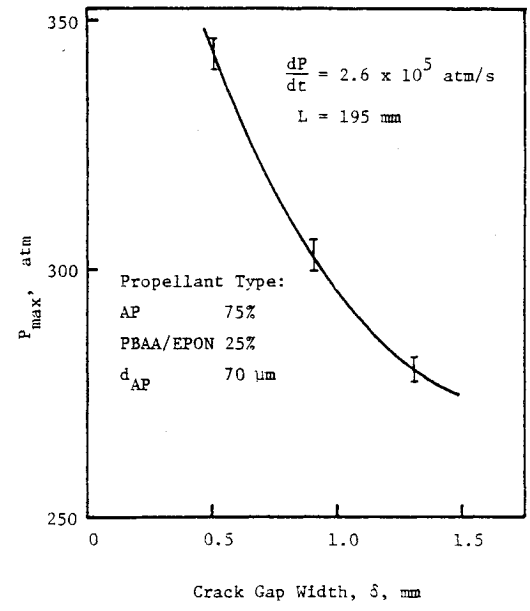

Fig. 11 Effect of gap width on maximum pressure in the crack.

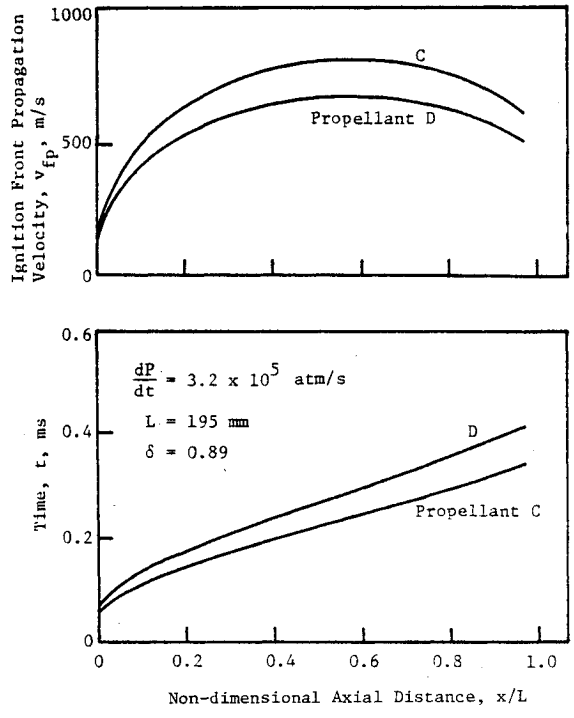

Fig. 12 Effect of burning rate on measured ignition front propagation.

tively. It is important to note that the effect of dP/dt, as depicted in Fig. 9, is valid only for the range of values indicated. As observed earlier by the authors,[6] under very high dP/dt conditions the crack tip may ignite before the ignition front propagates to the tip.

The effect of gap width on instantaneous location and velocity of the ignition front for propellant B is shown in Fig. 10. The length of the crack is 195 mm, and the crack-gap widths are 0.508, 0.889, and 1.27 mm. As the crack-gap width is increased, the ignition front penetrates the crack more quickly and reaches the tip sooner because the larger gap width offers less resistance to the penetration of the flow into the cavity. However, maximum velocity increases as the gap width decreases. This may be explained as follows. Since the time delay required for the ignition front to establish itself near the crack entrance is longer for cracks with smaller gap widths, the preheating effect caused by convective heat transfer is more pronounced. Once gasification begins, pressure behind the ignition front (due to gasification) will also be higher in narrow cracks. It is believed that the combined effect of preheating and higher pressure causes the ignition front to accelerate relatively rapidly in narrow cracks.

Figure 11 shows the effect of gap width on maximum pressure within the crack cavity. It is clear that as the gap width decreases, the maximum pressure in the cavity increases. As discussed earlier, maximum pressure in the crack cavity is determined by ignition and combustion processes inside the crack. Since crack depths are identical for all samples (25.4 mm), burning surface areas will also be identical as long as crack lengths for all samples are the same. As gap width is decreased, the burning surface area remains constant, but the opening area of the crack and volume of the crack gap decrease; therefore, maximum pressure is higher for smaller gap widths.

The effect of the burning rate on ignition-front propagation was studied by comparing results of tests conducted on propellants C and D as shown in Fig. 12. The initial crack length and gap width were 195 and 0.89 mm, respectively; the initial chamber pressurization rate was 3.2×10^5 atm/s. This comparison shows that the ignition-front propagation rate is faster for propellant C with its higher burning rate (AP particle size ~ 20 μm), than it is for propellant D with its lower burning rate (AP particle size ~ 200 μm). In these tests the effect of surface roughness was somewhat suppressed during the ignition-front propagation period because of the fact that surfaces were machined. The rate of flame propagation for a propellant with a higher burning rate is faster because the high burning rate produces more gases behind the ignition front and causes the local pressure gradient near the front to increase.

The effect of propellant type was investigated further by comparing the results of high-energy propellant A with those of propellant B. Even though both are AP-based propellants, the flame temperature and burning rate of propellant A are much higher than those of propellant B. Figure 13 shows a comparison of the ignition-front propagation rates of the two propellants. The crack samples were 195 mm long, with a gap width of 0.89 mm. The initial chamber pressurization rate was 3.2×10^5 atm/s. The more energetic propellant A has a shorter flame-spreading period and a higher maximum ignition-front velocity. Besides having a higher burning rate,

Table 2 Effect of propellant burning rate on P_{max}

	Propellant	Burning rate at 150 atm, mm/s	P_{max}, atm
$dP/dt = 3.2 \times 10^5$ atm/s	B	7.5	322
	D	8.9	334
$L = 195$ mm	C	12.7	354
$\delta = 0.89$ mm	A	14.0	371

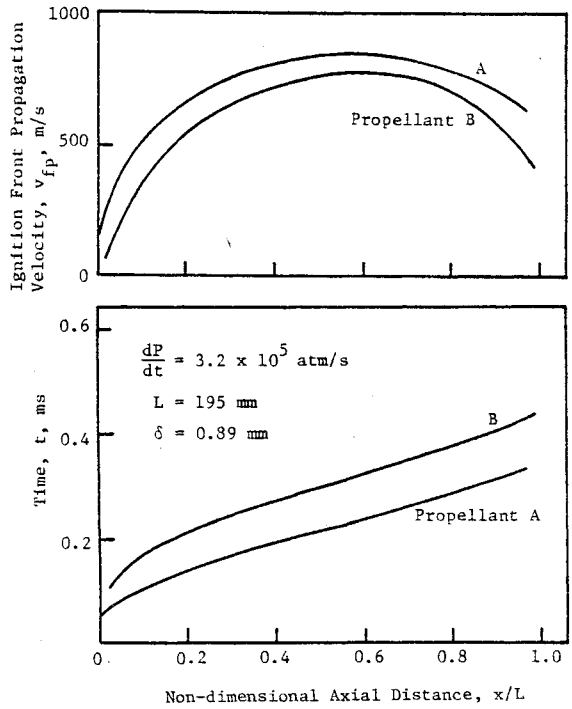

Fig. 13 Effect of propellant type on measured ignition front propagation.

the product gases generated from propellant A also have a higher temperature which further facilitates the ignition-front propagation process. Table 2 shows the effect of propellant burning rate on maximum pressure in the cavity. As the burning rate is increased, the maximum pressure in the crack also increases because higher burning rate propellants generate more gases, and for cracks of identical initial length and width (i.e., same initial volume of the crack cavity), this results in higher pressure.

Figure 14 shows the effect of crack length on ignition-front velocity. Propellant B was used in these tests, and the gap width was kept constant at 0.89 mm. The crack lengths were 65, 130, and 195 mm. As the crack length is increased, the time required for the ignition front to reach the crack tip increases, and the average ignition-front propagation velocity also increases. The times required for reaching the tip are 252, 476, and 511 μs, and the maximum ignition-front velocities are 435, 530, and 675 m/s for crack lengths of 65, 130, and 195 mm, respectively. Maximum pressure in the crack also increases as the crack length is increased. Higher flame-propagation velocities for longer cracks are the result of the reduced end effects which allows the flame front to accelerate. The ignition delay near the entrance portion of the crack is greater, however, for longer cracks. This may be the result of crack entrance deformation caused by pressure exerted on the front end of the crack sample. In general, these observations are in agreement with the limited data reported by Bobolev et al.[12]

In order to observe hot gas penetration and ignition-front propagation processes in detail, experiments were conducted using the alternate crack configuration (see Fig. 3). Figure 15

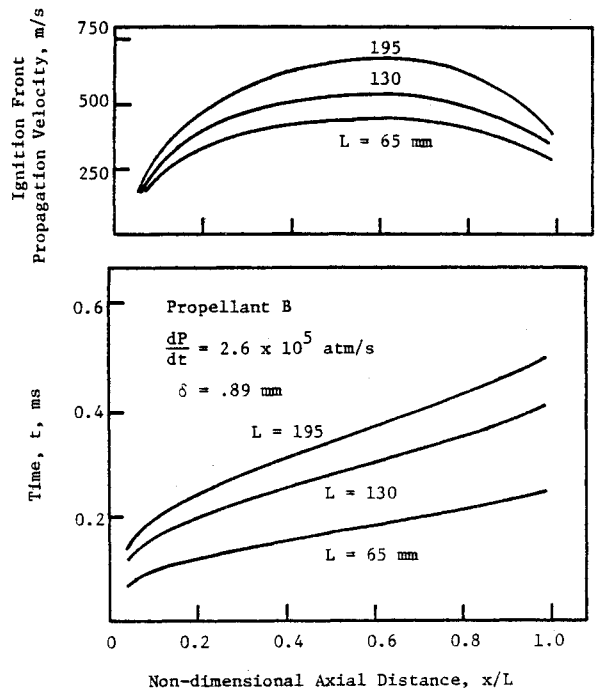

Fig. 14 Effect of crack length on measured ignition front propagation.

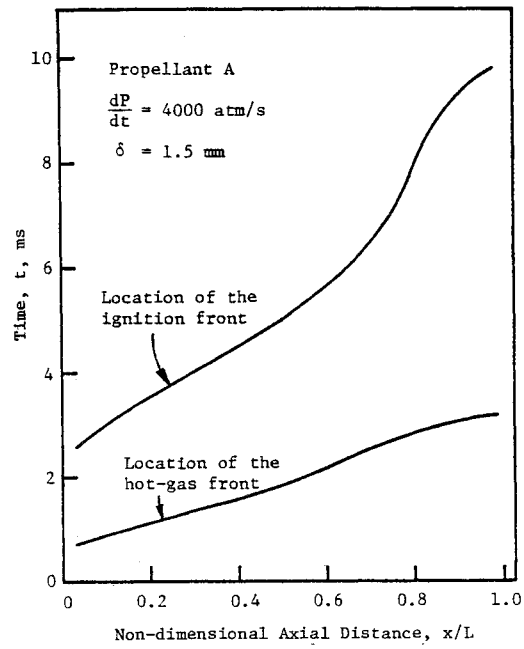

Fig. 15 Time history plot of hot-gas front location and ignition front location.

shows a typical time history plot of the hot gas front location and the ignition front. The pressurization rate for this case was 4000 atm/s, and the crack gap was 1.5 mm. A low pressurization rate was used in this test in order to detect the hot gas front clearly. It was observed that 1) the hot gases precede the ignition front along the crack and reach the tip much earlier than the convective ignition front; 2) the hot gases near the crack tip are luminous for a short period of time, with luminosity disappearing later (this can be attributed to the quenching of the hot gases); and 3) the flame front is nonuniform near the crack entrance, but becomes quite uniform as it propagates along the crack. The nonuniformity of the flame front near the crack entrance region can be attributed to the nonuniform flow at the entrance of a rectangular cross-sectional crack cavity.

Summary and Conclusions

The development of convective burning in an isolated crack has been studied experimentally under a wide range of operating conditions and propellant geometries. Four types of AP-based composite solid propellant were studied. A solid propellant igniter system was developed to closely simulate actual rocket conditions. A high-speed motion picture camera was used to measure the flame propagation rate. Several important observations and conclusions from this study are summarized as follows.

1) The initial pressure distribution in the crack is controlled by the chamber pressurization rate; however, the maximum pressure in the crack cavity is controlled by the initial crack geometry and the ignition and combustion processes in the crack.

2) The hot gases precede and reach the crack tip sooner than the ignition front. The ignition-front propagation speed increases near the crack entrance, reaches a maximum, and then decelerates near the closed end of the crack.

3) As the chamber pressurization rate or burning rate of the propellant is increased, the time required for the ignition front to reach the crack-tip decreases and the maximum flame-front propagation velocity increases.

4) As the gap width of the crack is decreased, the time required for the ignition front to reach the tip increases, but the maximum ignition-front propagation velocity also increases slightly. As the crack length is decreased, both maximum ignition-front propagation velocity and the time required for ignition front to reach the tip decrease.

5) The maximum pressure observed in the crack cavity increases when the gap width is reduced, when the crack length is increased, or when the propellant burning rate is increased.

Acknowledgments

A portion of the results reported in this paper were obtained under the research program sponsored by the Aerothermochemistry Division of the Naval Weapons Center, China Lake, California. The support and advice of Dr. R. L. Derr and Mr. C. F. Price are appreciated. Some of the results reported here were obtained under the project sponsored by the Power Program, Office of Naval Research, Arlington, Virginia, Contract N00014-79-C-0762. The support and advice of Dr. R. S. Miller is acknowledged. The assistance of J. E. Wills and D. Davies of The Pennsylvania State University is also acknowledged.

References

[1] Bradley, H. H. Jr. and Boggs, T. L., "Convective Burning in Propellant Defects: A Literature Review," Naval Weapons Center, China Lake, Calif., NWC TP 6007, Feb. 1978.

[2] Belyaev, A. F., Bobolev, V. K., Korotkov, A. I., Sulimov, A. A., and Chuiko, S. V., *Transition from Deflagration to Detonation in Condensed Phases,* translated from Russian by Israel Program of Scientific Translations, Jerusalem, 1975.

[3] Kuo, K. K., Chen, A. T., and Davis, T. R., "Convective Burning in Solid-Propellant Cracks," *AIAA Journal,* Vol. 16, June 1978, pp. 600-607.

[4] Kumar, M. and Kuo, K. K., "Ignition of Solid Propellant Crack Tip Under Rapid Pressurization," *AIAA Journal,* Vol. 18, July 1980, pp. 825-833.

[5] Kuo, K. K., Kumar, M., Kovacic, S. M., Wills, J. E., and Chang, T. Y., "Combustion Processes in Solid Propellant Cracks," Annual Report (from The Pennsylvania State University) to the Naval Weapons Center, China Lake, Calif., 1979.

[6] Kuo, K. K., Kovalcin, R. L., and Ackman, S. J., "Convective Burning in Isolated Solid Propellant Cracks," Naval Weapons Center, China Lake, Calif., NWC TP 6049, Feb. 1979.

[7] Kuo, K. K., McClure, D. R., Chen, A. T., and Lucas, F. G., "Transient Combustion in Solid Propellant Cracks," Naval Weapons Center, China Lake, Calif., NWC TP 5943, Oct. 1977.

[8] Prentice, J. L., "Flashdown in Solid Propellants," U. S. Naval Ordnance Test Station, China Lake, Calif., NAVWEPS Rept. 7964, NOTS TP 3009, Dec. 1962.

[9] Prentice, J. L., "Combustion in Solid Propellant Grain Defects: A Study of Burning in Single- and Multi-Pore Charges," Naval Weapons Center, China Lake, Calif., NWC TM 3182, June 1977.

[10] Margolin, A. D. and Margulis, V. M., "Penetration of Combustion into an Isolated Pore in an Explosive," *Combustion, Explosion, and Shock Waves,* Vol. 5, No. 1, 1969, pp. 15-16.

[11] Godai, T., "Flame Propagation into the Crack of Solid Propellant Grain," *AIAA Journal,* Vol. 8, July 1970, pp. 1322-1326.

[12] Bobolev, V. K., Margolin, A. D., and Chuiko, S. V., "The Mechanism by which Combusion Products Penetrate into the Pores of a Charge of Explosive Material," *DokLady Akademii Nauk USSR,* Vol. 162, May 1965, pp. 388-391.

[13] Payne, C. E., "Flame Propagation in Propellant Cracks," Air Force Rocket Propulsion Laboratory, AFRPL-TR-69-66, 1969.

[14] Krasnov, Y. K., Margulis, V. M., Margolin, A. D., and Pokhil, P. F., "Rate of Penetration of Combustion into the Pores of an Explosive Charge," *Combustion, Explosion, and Shock Waves,* Vol. 6, No. 3, 1970, pp. 262-265.

[15] Belyaev, A. F., Korotkov, A. I., Sulimov, A. A., Sukoyan, M. K., and Obmenin, A. V., "Development of Combustion in an Isolated Pore," *Combustion, Explosion, and Shock Waves,* Vol. 5, Jan.-March 1969, pp. 4-9.

[16] Belyaev, A. F., Bobolev, V. K., Korotkov, A. I., Sulimov, A. A., and Chuiko, S. V., "Development of Burning in a Single Pore," *Transition of Combustion of Condensed Systems to Detonation,* Chap. 5, Pt. A, Sec. 22, Science Publisher, 1973, pp. 115-134.

[17] Kumar, M., "A Study of Flame Spreading and Combustion Processes in Solid Propellant Cracks," Ph.D. Thesis, The Pennsylvania State University, Aug. 1980.

[18] Taylor, J. W., "The Burning of Secondary Explosive Powers by a Convective Mechanism," *Transactions of the Faraday Society,* Vol. 58, 1962, pp. 561-568.